# Durable Camouflage Materials by Polyimide Nanofilm with Thermal Management

Namkyu Lee[a], Joon-Soo Lim[b], Juyeong Nam[b], Hyung Mo Bae[b], Hyung Hee Cho[b†]

a. IBI-4, Forschungszentrum Jülich GmbH, 52425 Jülich, Germany

b. Department of Mechanical Engineering, Yonsei University, 50 Yonsei-ro, Seodaemun-gu, Seoul 13722, Korea

† Corresponding author

Tel.: +82 2 2123 2828

Fax: +82 2 312 2159

E-mail: hhcho@yonsei.ac.kr

## Abstract

Durable micro-nano structures are a crucial issue to protect their superior performance from external forces. Although several methods have been suggested to enhance the mechanical durability of micro-nano structures, they are not applicable for camouflage materials to obtain the wanted properties because these methods usually induce undesired resonances and severely reduce the radiative performance. The polyimide nanofilm with great mechanical properties can improve camouflage performance in camouflage materials with increasing the energy dissipation. Additionally, the polyimide nanofilm can be used as a transparent layer based on Beer-lambert's law. These characteristics indicate that the polyimide nanofilm can also be used to protect the micro-nano structures in camouflage materials. Herein, we propose durable camouflage materials for infrared waves with radiative cooling by coating the polyimide nanofilm on the structures. We realize the metal-dielectric-metal-nanofilm structures for the infrared camouflage. Spectral emissivity of durable camouflage materials via measurement and simulation satisfies the requirement for IR camouflage materials. The mechanical durability of proposed camouflage materials is verified by brushing and root cause analysis (RCA) test through visible and scanned electron microscope images. We evaluate that durable camouflage materials maintain their IR camouflage performance factor despite mechanical stress compared to the significant decrease in the performance factor of ordinary camouflage materials.

**Keywords**: *Camouflage materials; Mechanical durability; Polyimide nanofilm; Micro-nano structure; Radiative cooling;*

## 1. Introduction

Camouflage is an instinct behavior of creatures that blends themselves in with their surroundings, which enhances their survivability against predators.[1] Through learning from this nature's behavior, artificial camouflage materials are emerging fields, which can realize the designed the electromagnetic properties in acoustics,[2] microwave,[3–6] infrared (IR) wave,[7–9] visible,[10–12] and ultraviolet (UV) light,[13] depending on applications. In particular, IR wave is an emerging field because it is the center of energy and military applications such as thermophotovoltaics,[14,15] thermal management,[16,17] and stealth technology.[18–23]

IR wave can be controlled through temperature or surface emissivity based on the following relation,[24] $q'' = \varepsilon\sigma(T_s^4 - T_{surr}^4)$ with the heat flux q, the surface emissivity ε, the Boltzmann constant σ, the surface temperature $T_s$, the surrounding temperature $T_{surr}$, respectively. Although controlling the temperature is the intuitive way by thermoelectric devices enabling dynamic control depending on the surrounding condition,[25–28] they need the electrical apparatus to induce temperature variation. Hence, regulation of the surface emissivity is helpful to compensate for this disadvantage, because it does not require additional apparatus and can fabricate the thin film for arbitrary surfaces.[19,21,29–31]

There are two requirements for IR camouflage through the emissivity control: 1) low emissivity in detected bands (3 μm–5 μm and 8 μm–14 μm) and 2) high emissivity in undetected band (5 μm–8 μm).[19,31–34] IR camouflage is performed against the IR detector which operates in both bands, i.e., 3 μm–5 μm and 8 μm–14 μm corresponding to the atmospheric window passing the light with the minimized absorption through the atmosphere.[35] Therefore, IR camouflage materials lead to low emissive energy through the detected bands. Additionally, the lowering radiative energy can induce thermal instability due to the accumulation of energy into the structure based on energy conservation.[36] It means that we need to dissipate the decreased radiative energy in the detected band through the undetected band which absorbs the large part of radiative energy in

the medium. In the atmosphere, the 5 μm–8 μm band has many of absorption peaks due to the carbon dioxide and water, leading to the low transmission along the light path. It means that the undetected band can be used to dissipate the accumulated energy. Several camouflage materials such as metal-dielectric-metal (MDM) structure,[19–21,29,32] multi-layers,[30,37] and grating surfaces[38,39] have been introduced based on micro-nano structures to satisfy this requirement of IR camouflage materials.

Micro-nano structures are promising structures to overcome the limits of conventional materials because they significantly increase the surface-to-volume ratio[40] and provide eccentric properties that cannot be achieved by composites[41,42]. However, the micro-nano structures are fragile against mechanical stress, which can reduce the material performance abruptly and can be hard to use in actual applications.[43] There are several strategies such as chemical treatment, multiple hierarchical structures and coatings, to solve the poor durability.[44] It is difficult to use typical methods directly to enhance the durability in case of manipulating electromagnetic waves because the optical properties are so sensitive to induce the additional resonances and opaqueness in the target wave that differ the optical performance despite thin films. The polyimide nanofilm for a dielectric layer in IR camouflage materials because of its flexibility and anomalous dispersions in the undetected band (5 μm–8 μm) satisfying the IR camouflage requirement[29]. Polyimide is a well-known material for its excellent mechanical property and thermal stability.[45] We conclude, based on these characteristics and optical properties, that the polyimide nanofilm can enhance mechanical durability via coating on the structures.

Herein, this paper introduces the durable camouflage materials for IR camouflage. We coated the polyimide nanofilm on ordinary metal-dielectric-metal (MDM) structures to enhance mechanical durability. We verified the IR camouflage performance of durable camouflage materials using measurement (Fourier transform infrared spectroscopy (FT-IR)) and simulation (COMSOL Multiphysics). We demonstrated the enhanced mechanical durability compared to ordinary camouflage materials through two methods—brushing by hand

and the root cause analysis (RCA) test. Finally, We evaluated the IR camouflage factor[19] and conclude that the IR camouflage performance based on energy dissipation calculation and an infrared image did not change before and after the mechanical stress.

## 2. Research details

### 2.1. Fabrication

The silicon wafer with 500 μmt thickness was prepared as a substrate after cleaning the surface with acetone, ethanol, and buffered-oxide etchant (BOE) to remove organic matters on the wafer sequentially. On the cleaned wafer, VTEC 1388 (liquid polyimide) makes a 13 μm thickness layer with 3000 rpm. After that, Au/Ti-$SiO_2$/Au layers were deposited on the polyimide layer using the electron beam evaporator (E-beam evaporator, ULVAC, Japan) for metal and plasma enhanced chemical vapor deposition (PECVD, Plasmalab 800 Plus, Oxford Instruments, UK) for a dielectric disk. Au with 100 nm thickness as a metal layer and Ti with 10 nm thickness as an adhesive layer were used to enhance the compatibility between Au and other layers. The adhesive layer usually does not affect the spectral emissivity in the MDM structure.[46] The thickness of $SiO_2$ was 150 nm. The photoresist (AZ5214E, Microchemicals, Germany) was coated for 30 s at 3000 rpm and an EVG aligner (wavelength = 365 nm) was used for patterns. MIF-300 (developer) was used to develop the patterns after photolithography on the deposited surface. After that, inductively coupled plasma etching (ICP, PlasmaPro 800 RIE, Oxford Instruments, UK) was utilized to make the disk of the top metal and dielectric materials. The remaining photoresists on the surface were then removed by a plasma asher (100 W, 5 min). We coated the nanofilm of a thickness below 500 nm n the fabricated surface. We used solvent (N-Methyl-2-pyrrolidone (NMP)) with a volume ratio of 1:1.5 to reduce the viscosity of VTEC 1388. The variation in the film thickness is described in the Supporting information (Figs. S1 and S2). We then additionally coated the fabricated surface with the diluted mixtures (3000 rpm, 30 sec), inducing the film thickness of 130 nm. The actual film thickness was 300 nm, owing to the solution between disks. The final structure is presented in Figs. 1b and c.

## 2.2. Simulation

We performed the simulation with a commercial code, COMSOL Multiphysics v.5.2.a including an optics module to analyze the electromagnetic behaviors in durable camouflage materials. The governing equation, Maxwell's equation, was used by the discretization for a finite element method. We assumed the infinite surface consisting of durable camouflage materials utilizing the periodic boundary condition. The simulated domain was composed of a metal ground, dielectric disk, metal disk, nanofilm and medium. The variables were the diameter (d) of the dielectric and the metal disk and the pitch (p), which were chosen to distinguish between the types of magnetic resonances and the wavelength change. The relative permittivity, permeability, and electrical conductivity in the medium were 1, 1, and 0, respectively, which were assumed as the vacuum. The free electron behavior in the metal disk and ground is described by the Drude-Lorentz dispersion model with the plasma frequency (2.06 PHz) and the damping constant (13.34 THz) of Au in the simulation.[19] The optical properties of $SiO_2$ were used by the manipulated refractive indexes[47] fitted with the experimental result because of the discrepancy in simulated results. The target wavelength range was 3 μm−14 μm; the number of grids was approximately 100000, determined by the grid-independent test.

## 2.3. Measurement of Infrared Emissivity

FT-IR (Bruker Corp.) was utilized to measure the spectral emissivity of the specimen.[19–21,29,32] The wavelength range of 1.3 μm − 27 μm was measured using a beam splitter (KBr) to induce phase difference. The reflectivity was measured using the reflection accessory (Bruker A513) based on Kirchhoff's law as follows: $\varepsilon(\lambda) = \alpha(\lambda) = 1-\rho(\lambda)$ with emissivity ε, absorptivity α, reflectivity ρ and wavelength λ, respectively. The transmittivity was assumed as zero because of the metal ground at the bottom of the materials. Based on the signal ratio between the reference and sample, the reflectivity was determined from this relation: $\rho(\lambda) = S_{sample}(\lambda,T) / S_{reference}(\lambda,T)$ with the reflected signal S and the temperature T, respectively. The temperature

was controlled using the air conditioning system. Moreover, the specimen size was below 1.3 cm x 1.3 cm. Furthermore, Au was used as a reference surface with a thickness of 200 nm, inducing the reflectivity of the unity.

### 2.4. Thermographic and Visible Measurement

The thermographic image was monitored by an IR camera (A655sc, FLIR Systems, Wilsonville, OR, US) to observe an infrared camouflage performance of the heated surface. Two specimens were measured based on the existence of polyimide nanofilm. The heated surface was induced by the heating plate; its temperature was set at 370 K (87°C), corresponding to the Mach number = 2.0 at the altitude of 5000 m.[24] Upon the heating plate, the polished copper plate existed to compare the IR signal in the same temperature condition. The processed emissivity of IR data was assumed as 0.95. The visible image was measured using the camera with the following specifications (12MP Dual Pixel, f/1.7, and 1.4-micron pixels OIS).

## 3. Results and Discussion

### 3.1. Strategy of Durable Infrared Camouflage Materials

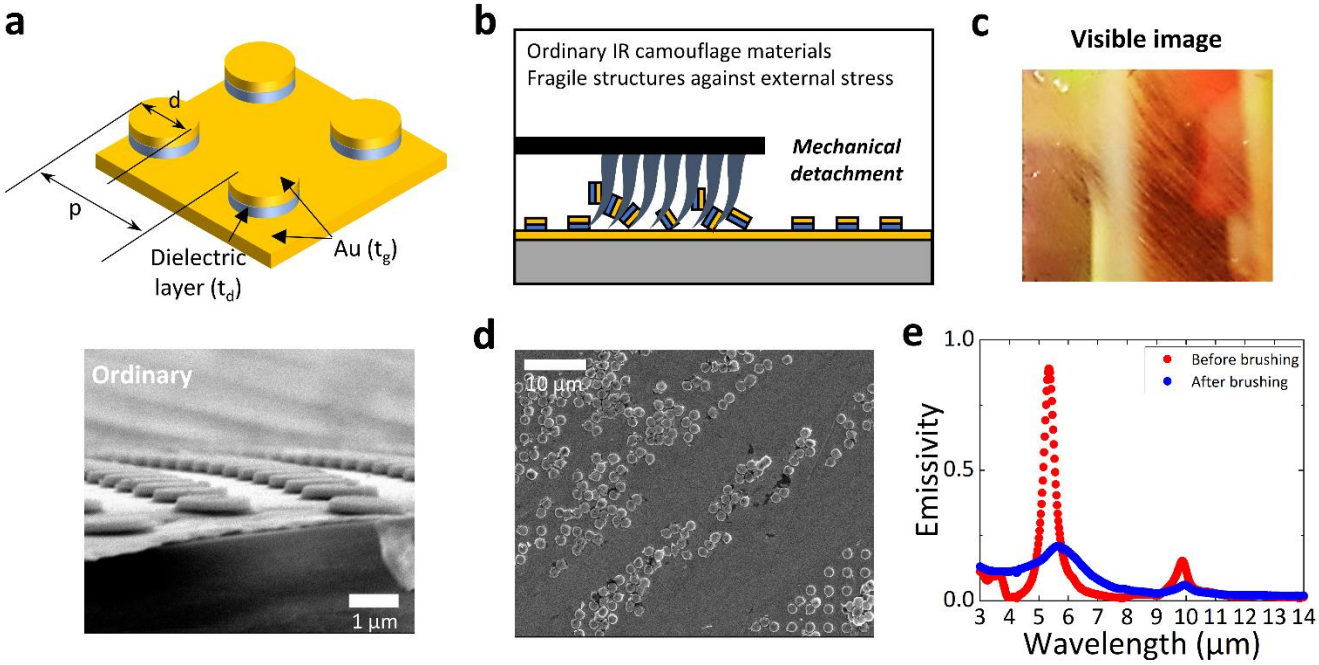


**Figure 1. a.** Schematic of ordinary camouflage materials for infrared wave. Ordinary camouflage materials consist of three parts: metal ground (Au), dielectric disk ($SiO_2$), and metal disk (Au). Diameter (d) and pitch (p) of durable camouflage materials were 1.45 μm and 3 μm, respectively. The thicknesses of $t_g$ and $t_d$ were 100 nm and 150 nm, respectively. The scanned electron microscopy (SEM) image shows the fabricated materials with a scale bar of 1 μm. **b.** Description of mechanical detachment on ordinary camouflage materials after inducing the mechanical stress on the surface. **c.** Visible and **d.** SEM images after brushing on the ordinary camouflage materials. **e**. Change in the spectral emissivity before and after brushing. The spectral emissivity shows that the selective emission disappears due to the destruction of camouflage materials.

Figure 1a shows the schematic of ordinary camouflage materials for IR wave. The ordinary camouflage materials are usually MDM structures.[19,20,32,48] Au is used as a metal ground and metal disk. Then, silicon oxide ($SiO_2$) is employed as a dielectric layer. The diameter and pitch of metal and dielectric disks are 1.45 μm and 3 μm, respectively. The thicknesses of Au/Ti and $SiO_2$ were 100/10 nm and 150 nm, respectively. The bottom SEM image in Fig. 1a shows the successful fabrication of camouflage materials.

Based on the ordinary camouflage materials, we used the brush by hand, which assimilates the cleaning process on the surface, for qualitative evaluation of the mechanical durability. The IR camouflage materials

are aimed at military and energy applications. They require periodic cleaning because their optical performance is easily affected by the residue on the surface.[49] For this reason, we need to evaluate the mechanical durability and guess if the external stress happens on the camouflage materials, then brushing leads to the destruction of camouflage materials shown in Fig. 1b.

Figure 1c shows our suspect through the visible image, indicating the destruction of fabricated materials. We found that brushing results in peeling structures and changes the gold to black. We observed the SEM image on brushed materials to perform a detailed inspection of structural destructions. Figure 1d shows the destroyed structures on the surface after brushing. Structures were ruined along the brushing direction, and only a few materials remained on the surface. It implies that ordinary camouflage materials cannot be protected against mechanical stress of the brush by hand.

We observed the change in the spectral emissivity due to brushing related to this destruction. Figure 1e shows that the spectral emissivity of materials before brushing satisfies the requirements of IR camouflage materials, low emissivity energy for low detection in the detected band (3 μm–5 μm and 8 μm–14 μm) and high emission for energy dissipation of accumulated energy through the undetected band (5 μm–8 μm). However, after brushing, the energy dissipation disappeared in the undetected band and only remained the low emission in whole IR range. If the metal ground disappears completely after brushing, then the spectral emissivity is larger than before because silicon substrate has larger emissivity than metal surfaces.[42] Since the low spectral emissivity in the entire regime was maintained, the Ti layer still attached on the surface and led to low emission. Moreover, destroyed materials also remain on the surface, which also acts as a reflector (see Fig. 1d). It implies that the energy accumulation due to lowering energy dissipation in the detected bands can lead to thermal instability in the system.[36] Therefore, it shows that the ordinary camouflage materials exposed by mechanical stress of the brush do not satisfy the requirement of IR camouflage.

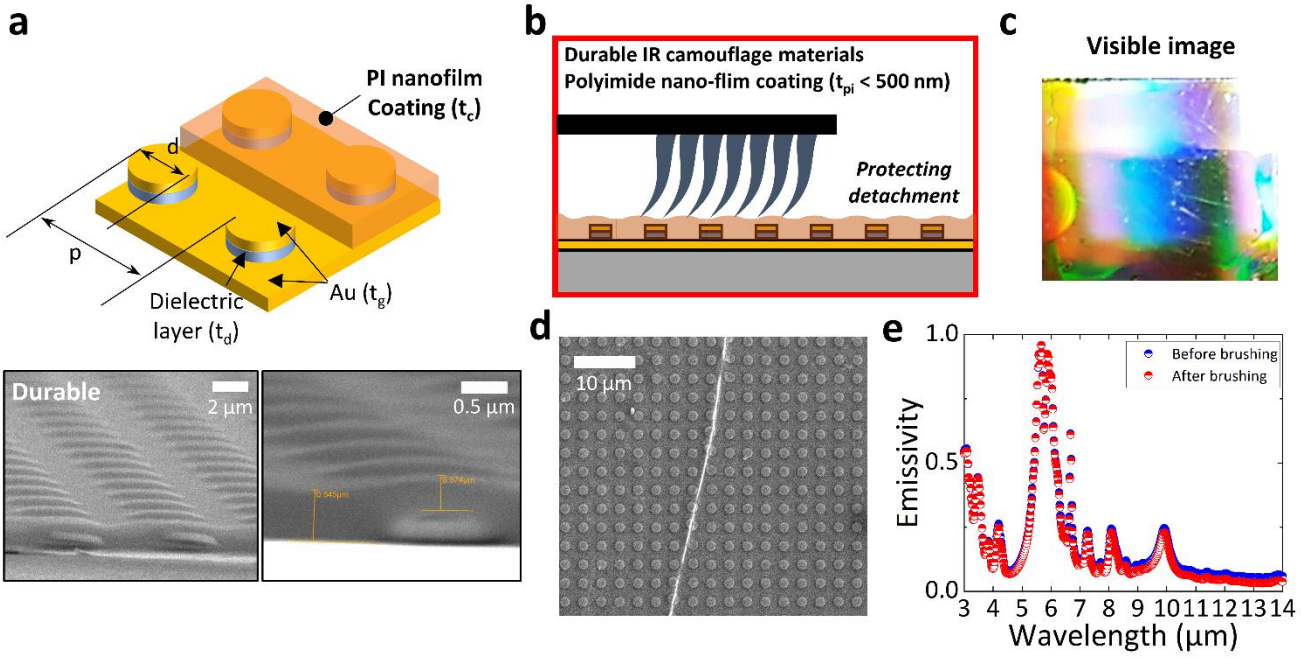


**Figure 2. a.** Schematic of durable camouflage materials for infrared wave. Durable camouflage materials consist of four parts: metal ground (Au), dielectric disk ($SiO_2$), metal disk (Au) and polyimide (PI) nanofilm. Diameter (d) and pitch (p) of durable camouflage materials were 1.45 μm and 3 μm, respectively. Their thicknesses of $t_g$ and $t_d$ are 100 nm and 150 nm. The thickness of PI nanofilm ($t_c$) was 358 nm. SEM images of durable camouflage materials show fabricated materials. The image shows the durable camouflage materials covered by the nanofilm. **b.** Description of the surface protection due to the PI thin-film coating against mechanical detachment after inducing the mechanical stress on the surface. **c.** Visible image and **d.** SEM images after brushing on the durable camouflage materials, showing the PI nanofilm that protects the camouflage materials sufficiently. **e**. Change in the spectral emissivity before and after brushing. The spectral emissivity demonstrates that the PI nanofilm protects the camouflage performance.

Figure 2a shows the schematic of the unit cell in durable IR camouflage materials. The polyimide nanofilm was employed for protecting camouflage materials to improve their durability against mechanical stress. There have been several studies on self-cleaning surfaces to enhance the mechanical durability of micro-nano structures against external stresses.[44] They have attempted to fix the root of the micro-nano structure, enhancing the adhesion between structure and substrate. Otherwise, they coat additional materials to keep the surface properties as required. In case of camouflage materials for enhancing the mechanical durability, we should consider optical properties in the IR wave additionally. In general, many materials have optical opaqueness because of many of unwanted resonances in the target wavelength range. However, if the

transparent thin film can be fabricated, then it is also possible to use any materials to improve mechanical durability. We already note that every material can be transparent when the thickness of the material is sufficiently thin based on the Beer-Lambert law expressed as $I(z) = I_0 \exp(-z/\alpha)$ with the light intensity I, the optical path z, and the absorption coefficient α, respectively.[50] Moreover, if the additional resonances due to the coating material help to increase the camouflage performance, then we can use the coating material for protecting structures. In the previous research, we already utilized the polyimide nanofilm as a dielectric layer because the molecular resonances of polyimide are helpful in enhancing the energy dissipation in the undetected band (5 μm–8 μm) and to maintain the transparent behaviors in the detected bands (3 μm–5 μm and 8 μm–14 μm). Therefore, we found that the PI nanofilm over the ordinary camouflage materials can protect the camouflage materials, as shown in Fig. 2b. The bottom images in Fig. 2a show the scanned electron microscopy (SEM) image. We observed that durable IR camouflage materials were covered with PI nanofilm compared to ordinary IR camouflage materials. The measured thickness of nanofilm ($t_c$) was 358 nm.

Figure 2c shows the visible image of durable camouflage materials after brushing the surface. It is difficult to find scratches on the surface compared to the ordinary camouflage materials, implying that structures are protected by the polyimide nanofilm from external stress. We also investigated SEM images and spectral emissivity depending on brushing to demonstrate the enhanced durability against the mechanical durability in detail. Figure 2d shows the SEM image after brushing on the materials. We found that the structures were retained after brushing. Especially, SEM image proves that structures on scratches even endure the mechanical stress entirely, even though brushing deteriorates the structure of ordinary camouflage materials (Fig. 1d). Furthermore, durable materials do not change the spectral emissivity before and after brushing. As shown in Fig. 2e, the spectral emissivity satisfies the following requirements of IR camouflage despite brushing on materials: low emissivity in detected bands and the high emissivity in the undetected. Additionally, the change in the spectral emissivity depending on brushing is negligible, which means that the nanofilm can protect the

camouflage materials sufficiently. These results show that the durable camouflage materials with nanofilm can protect materials from mechanical stress as well as satisfy the requirement of IR camouflage simultaneously. We further analyzed the detailed optical characteristics and mechanical durability based on these results.

### 3.2. Optical and Mechanical Performance of Durable Camouflage Materials

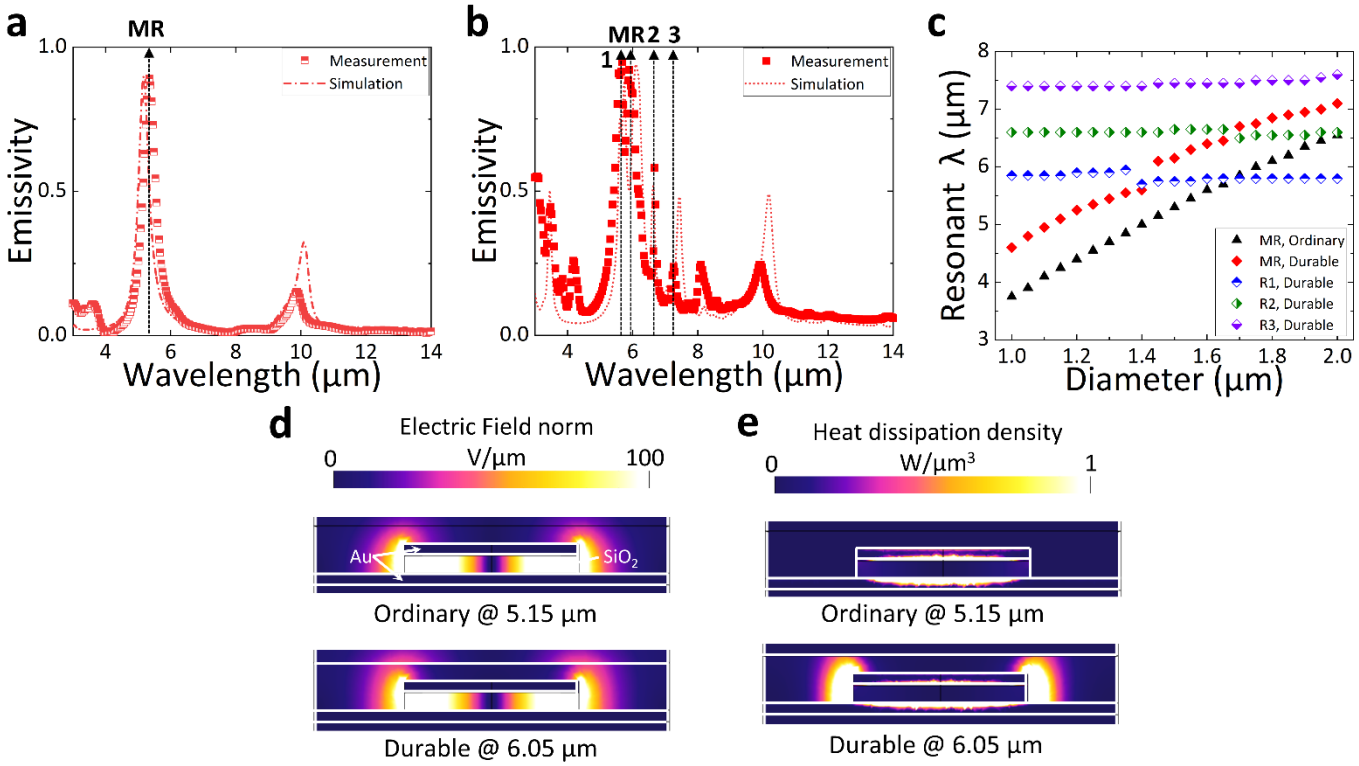


**Figure 3.** Spectral emissivity depending on **a.** ordinary and **b.** durable camouflage materials. Several resonances are seen between 5 μm and 8 μm due to the resonances by lattice vibration in the nanofilm. **c**. Variation in the resonant wavelength depending on metal disk diameter, which helps to distinguish the localized and non-localized plasmonic behaviors in materials. Distribution of **d.** electric field norm and **e.** heat dissipation density of ordinary and durable camouflage materials at 5.15 μm and 6.05 μm, respectively.

We measured the spectral emissivity with fabricated materials to test if durable camouflage materials can be used as IR camouflage materials. Figure 3a and b show the spectral emissivity of ordinary and durable IR camouflage materials, respectively. The low emissivity for the IR camouflage happens in the detected band (3 μm–5 μm and 8 μm–14 μm), reducing the signal from the surface. Moreover, the high emissivity occurs in the undetected band (5 μm–8 μm) which dissipates the reduced energy in the detected bands. As shown in Fig. 3a, ordinary camouflage material satisfies the requirement of IR camouflage materials. Durable IR camouflage materials had several small peaks after coating the nanofilm on ordinary camouflage materials. However, it satisfied the requirement of IR camouflage materials. We need to simulate and compare electromagnetic

behaviors of the ordinary and durable IR camouflage materials to understand the effect of the nanofilm coating on spectral emissivity. In Fig. 3a and b show that the simulation agrees with the measurement, which shows that the simulation can be used as an analyzing tool in this study.

To distinguish the types of resonances in the IR range, we analyze the change in the resonance wavelength depending on the disk diameter (d), as shown in Fig. 3c. The resonances in the MDM structure depend on geometrical factors, such as diameter (d) and pitch (p).[51] If the resonance wavelength depends on the disk diameter, the resonance is treated as a localized plasmonic behavior. However, if it depends on the pitch, then this resonance is characterized as a non-localized plasmonic behavior. These behaviors cannot happen simultaneously, meaning that the localized and non-localized plasmonic behaviors are independent of the pitch and diameter, respectively. Figure 3c shows the resonant wavelength depending on the change in the diameter having a silicon oxide. We observe by comparing the Fig. 3a, b and c that magnetic resonance (MR) is dependent on d. However, additional resonances (1, 2, and 3) with the polyimide nanofilm coating are independent of d. It means that MR can be classified as the localized plasmonic behavior and the other resonances due to the anomalous dispersion in polyimide[52] can be considered as the non-localized plasmonic behavior. Moreover, when the magnetic resonance is shifted, the strength of other resonances due to anomalous dispersion increases in Fig. 3b and c. When the magnetic resonance with silicon oxide happens around 6 μm, the resonance due to lattice vibration of nanofilm induces the unity emissivity around 5.8 μm (Fig. 3b). It shows that the lattice vibration in the nanofilm interacts with the magnetic resonance in the structure.

In addition, we visualize the electric field and heat dissipation using the simulation to analyze the electric field in the structure depending on the nanofilm coating. We indirectly analyze the electromagnetic behavior of the emission through the absorption because the emissivity and absorptivity are the same in the thermal equilibrium.[24] Figure 3d and e show the electric field and the heat dissipation density in the structure of ordinary and durable camouflage materials, respectively. As shown in Fig. 3d, the electric field is similar

irrespective of camouflage material types qualitatively, meaning that the high emissivity is not caused by varying the electric field due to the nanofilm. Figure 3e presents the heat dissipation density in the structure which can show the causing part of high emissivity (absorptivity) in the structure. The heat dissipation is confined in the gold parts of ordinary camouflage materials, which is usually caused by the joule dissipation in the metal parts.[53] However, the significant amount of heat dissipation additionally happens in the nanofilm of durable camouflage materials similar to the pattern of the electric field (Fig. 3d). It means that the nanofilm interacts with the electric field and induces additional resonances. We note that, if the nanofilm without anomalous dispersion in the IR regime can be used, then the additional resonances due to the lattice vibration of the nanofilm can be removed.

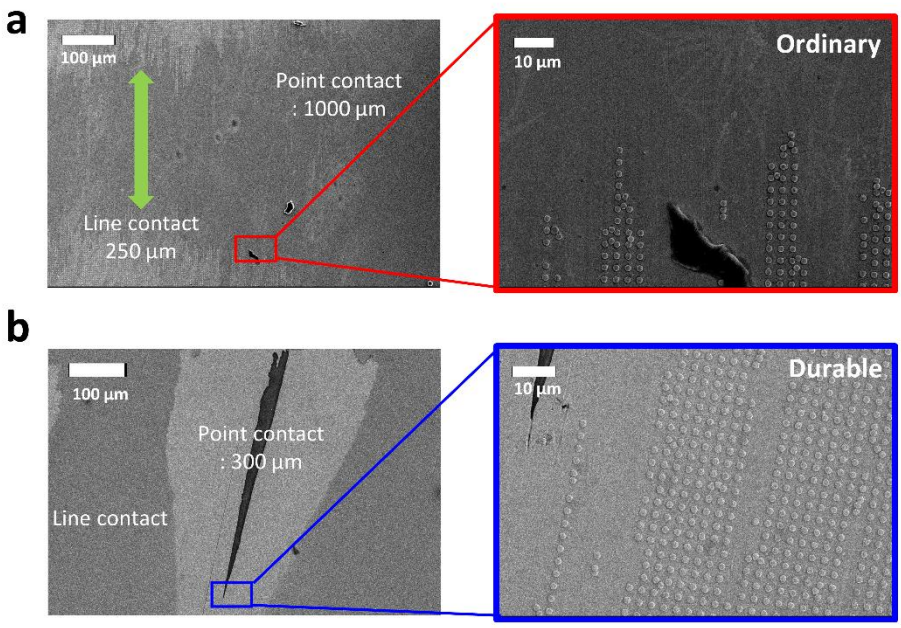


**Figure 4. a**. SEM image of ordinary camouflage materials after RCA test. The area of brighter color indicates the remained structures, and the darker color means the destroyed area due to mechanical stress. Every contact (point and line) damages the structure. **b.** SEM image of durable camouflage materials after RCA test. Except for point contact, the structures against line contact remain under mechanical stress.

For the evaluation of mechanical durability further, we used RCA with paper for abrasion on the surface to check the protection quantitatively. The detailed information on RCA with paper is provided in the Supporting information (Fig. S5). There were two contacts performed by RCA tests: point and line contact. The highest averaged pressure (450 kPa) was experienced at the point contact, with a much larger value than the general hand contact on the surface.[54] The line contact was caused by the friction of paper around the contact point. It is difficult to calculate the exact value. However, this value is much smaller than the point contact because the line contact is not directly pressurized by the pointer. The ordinary camouflage materials in Fig. 4a show that both contacts deteriorated structures on the surface entirely. Moreover, the spallation at the contact point happened, and the line contact between structures and paper also destroyed structures. It means that the structure is very fragile against external stress even though the contact pressure at the line contact is much lower than the point contact. However, Fig. 4b demonstrates that structures under the nanofilm coating were

protected except for the contact point. Particularly, though the structure disappeared and the spallation happened at the contact point, structures still remained along the line contact, contrary to the ordinary camouflage materials. We recognized that the durable IR camouflage materials endures more at least half of contact pressure based on the SEM image after brushing and the RCA test.

### 3.3. Infrared Camouflage Performance of Materials

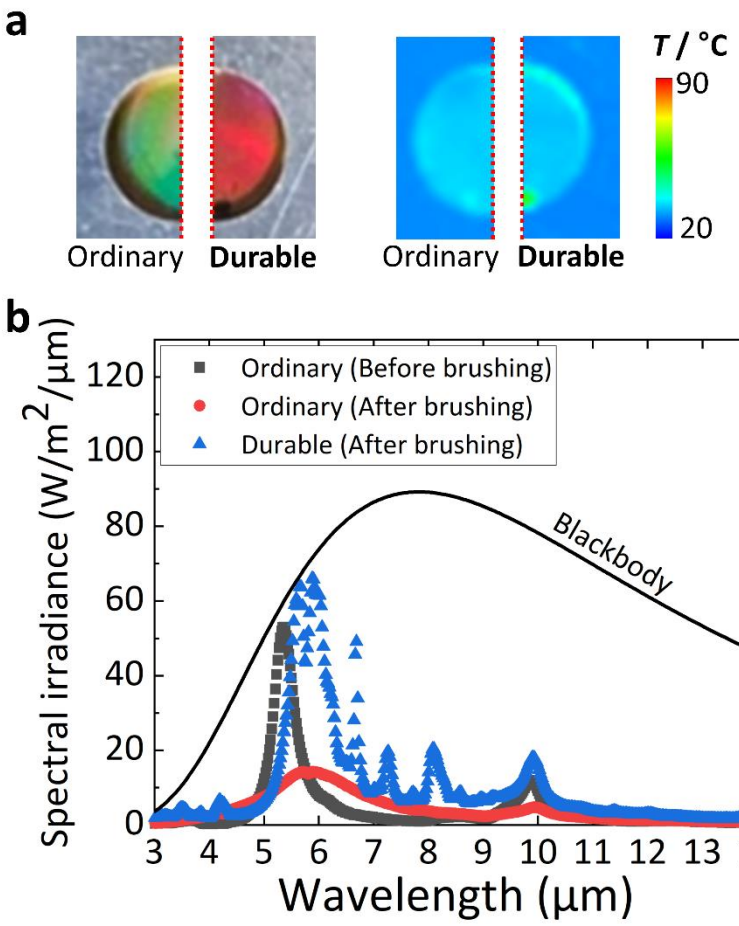


**Figure 5. a**. Comparison of visible and infrared images between ordinary and durable camouflage materials. The difference in apparent temperature via infrared camera is negligible due to the insignificant impact of polyimide nanofilm. **b**. Spectral irradiance of a blackbody, ordinary camouflage materials before and after brushing, and durable camouflage materials after brushing. Spectral irradiance of durable camouflage materials is not affected by external stress.

We evaluated the apparent temperature of the surface compared to the heated temperature, and calculated the radiative energy compared to the reference surfaces to evaluate the IR camouflage performance. Figure 5a shows the visible and IR images of ordinary and durable camouflage materials. The temperature of the heated plate was set at 87°C, which value targets the total temperature calculated by the high-speed aircraft of Mach number = 2.0 at the altitude of 5000 m. The amount of reducing the apparent temperature by ordinary camouflage materials (34.5°C) was 52.5°C. Such amount of that temperature by durable camouflage materials

(34.7°C) is 52.3°C. The difference in reducing the temperature by durable camouflage materials was negligible depending on the nanofilm. It shows that the camouflage performance in the detected band (8 μm–14 μm) remained constant regardless of the nanofilm. Additionally, the reduction in apparent temperature by copper plate (28.1°C) was 58.9°C, which amount is similar to the camouflage materials (52.3°C). It means that the durable camouflage materials are sufficient to hide the backside temperature from the heating plate. The reduced apparent temperature of durable camouflage materials was approximately the same as those without coating. Thus, we confirm that durable camouflage materials can be used as ordinary camouflage materials by enhancing mechanical durability.

Moreover, we quantified the variation of radiative energy in detected and undetected bands, because it is difficult to estimate the radiative energy from the operating range of the IR camera. When we hypothesize the diffusive emission from the surface, the spectral irradiance of blackbody can be calculated as following equation:[24]

$$E_{b\lambda}(\lambda, T) = \frac{2\pi h c_0^2}{\lambda^5 \left[\exp[\frac{hc_0/k}{\lambda T} - 1]\right]} \quad (1)$$

with the Planck's constant h, the speed of light in vacuum $c_0$, the Boltzmann's constant k and the surface temperature, respectively. We integrated the spectral irradiance along with wavelength to evaluate the radiative energy in the specific band. If the band ranges from $\lambda_1$ to $\lambda_2$, the result of integration is presented as follows:

$$E_{\lambda_1-\lambda_2}(T) = \int_{\lambda_1}^{\lambda_2} \varepsilon(\lambda, T)\, E_{b\lambda}(\lambda, T)\, d\lambda \cong \sum \varepsilon(\lambda, T)\, E_{b\lambda}(\lambda, T)\Delta\lambda \quad (2)$$

with the measured emissivity of materials ε.

Figure 5b compares the spectral irradiance depending on the ordinary camouflage materials before and after brushing, durable camouflage materials after brushing. We investigated the camouflage performance of camouflage materials compared to the blackbody. The radiative heat flux of ordinary camouflage materials

was 3.3 W/m$^2$ in 3 μm–5 μm and 14.4 W/m$^2$ in 8 μm–14 μm before brushing with emissivity of 0.07 and 0.03 in 3 μm–5 μm and 8 μm–14 μm, respectively. After brushing, the radiative heat fluxes of ordinary camouflage materials were 6.0 W/m$^2$ and 12.7 W/m$^2$ in 3 μm–5 μm and 8 μm–14 μm, respectively. These radiative heat fluxes cannot show the reduced camouflage performance due to the destruction of structures. However, the radiative heat flux of ordinary camouflage materials for energy dissipation in the undetected band 5 μm–8 μm changed from 32.9 W/m$^2$ to 27.5 W/m$^2$ with a decrease of 16% due to brushing. The radiative heat fluxes were 6.7 W/m$^2$ and 34.2 W/m$^2$ in 3 μm–5 μm and 8 μm–14 μm, respectively, which values are 0.14 of a blackbody in 3 μm–5 μm and 0.08 of a blackbody in 8 μm–14 μm. The radiative heat flux of durable camouflage materials for energy dissipation was 72.9 W/m$^2$, which is 265% larger than that of ordinary camouflage materials.

Based on these radiative energy relations, we calculated the camouflage performance factor with the reduced energy in detected bands and the enhanced energy dissipation in the undetected band[19] to compare this effect simultaneously; it is expressed as follows: CP = $\bar{\varepsilon}^2_{5-8\,\mu m}/(\bar{\varepsilon}_{3-5\,\mu m}\bar{\varepsilon}_{8-14\,\mu m})$. The camouflage performance factor of ordinary camouflage materials changed from 8.1 to 3.8 before and after brushing, implying that the significant destruction of structure on the material. The camouflage performance factor of durable camouflage materials after coating and brushing was from 8.1 to 8.6, which is 226% larger than that of ordinary camouflage materials. This larger value originates from the enhanced energy dissipation in the undetected band contrary to the ordinary camouflage materials' performance. Therefore, we conclude that durable camouflage materials can provide mechanical durability as well as IR camouflage performance for practical applications.

## 4. Conclusion

We propose durable IR camouflage materials by coating the nanofilm on the structures. Based on the Beer-Lambert law, we utilize that polyimide nanofilm can be used as a coating layer, which has little impact on the optical properties in the specific regime. The results of spectral emissivity show that durable IR camouflage materials satisfy the requirements of IR camouflage simultaneously with low emission in detected bands (0.14 in 3 μm–5 μm and 0.08 in 8 μm–14 μm) and high emission in undetected band (0.31 in 5 μm–8 μm). In particular, the enhanced energy dissipation happened in the undetected band due to the interaction between the polyimide nanofilm and the MDM structure. Moreover, we verified the significant enhancement of mechanical durability through brushing and RCA test compared to the ordinary camouflage materials. Especially, MDM structures in durable IR camouflage materials are protected against mechanical spallation, which induces identical spectral emissivity in the IR bands before and after the exposure of the mechanical stress. We demonstrate the IR camouflage performance through the IR image and calculation of radiative heat flux in the detected and undetected bands. Durable IR camouflage materials can maintain the camouflage factor through the integrated camouflage factor regardless of mechanical stress, unlike ordinary camouflage materials. We conclude that durable IR camouflage materials simultaneously provide mechanical durability and IR camouflage performance owing to coating the nanofilm on the structure. We could not achieve the ideal protection without changing the spectral emissivity due to the lattice vibration of the coating material; however, we realized durable IR camouflage materials using the optical properties of polyimide in the IR band. It means if we can develop the nanofilm without the lattice resonance in the IR band, then we may further advance durable IR camouflage materials. We believe that this study can be applied to various applications by protecting the metal-dielectric-metal structure, because the micro-nano structure is extremely fragile against mechanical stress. We hope that this study will be helpful in enhancing the durability of micro-nano structures for energy, military and space applications.

## Author Information


### Corresponding Author

*E-mail: hhcho@yonsei.ac.kr


## Acknowledgements


This work was supported by the Aerospace Low Observable Technology Laboratory Program of the Defense Acquisition Program Administration and the Agency for Defense Development of the Republic of Korea.

## References


[1] J.B. Barnett, C. Michalis, H.M. Anderson, B.L. McEwen, J. Yeager, J.N. Pruitt, N.E. Scott-Samuel, I.C. Cuthill, Imperfect transparency and camouflage in glass frogs, Proc. Natl. Acad. Sci. U. S. A. 117 (2020) 12885–12890. https://doi.org/10.1073/pnas.1919417117.

[2] T. Brunet, A. Merlin, B. Mascaro, K. Zimny, J. Leng, O. Poncelet, C. Aristégui, O. Mondain-Monval, Soft 3D acoustic metamaterial with negative index, Nat. Mater. 14 (2015) 384–388. https://doi.org/10.1038/nmat4164.

[3] C. Hou, J. Cheng, H. Zhang, Z. Lu, X. Yang, G. Zheng, D. Zhang, M. Cao, Biomass-derived carbon-coated WS2 core-shell nanostructures with excellent electromagnetic absorption in C-band, Appl. Surf. Sci. 577 (2022) 151939. https://doi.org/10.1016/j.apsusc.2021.151939.

[4] Z. Qu, Y. Wang, W. Wang, D. Yu, Hierarchical FeCoNiOx-PDA-rGO/WPU layers constructed on the polyimide fabric by screen printing with high microwave absorption performance, Appl. Surf. Sci. 562 (2021) 150190. https://doi.org/10.1016/j.apsusc.2021.150190.

[5] G. He, Y. Duan, H. Pang, X. Zhang, Rational design of mesoporous MnO2 microwave absorber with tunable microwave frequency response, Appl. Surf. Sci. 490 (2019) 372–382. https://doi.org/10.1016/j.apsusc.2019.06.037.

[6] F. Costa, A. Monorchio, G. Manara, Analysis and Design of Ultra Thin Electromagnetic Absorbers Comprising Resistively Loaded High Impedance Surfaces, IEEE Trans. Antennas Propag. 58 (2010) 1551–1558. https://doi.org/10.1109/TAP.2010.2044329.

[7] M. Zhang, G. Yang, Li Zhang, Y. Zhang, J. Yin, X. Ma, J. Wen, L. Dai, X. Wang, H. Chen, L. Zhang, L. Yin, X. Jian, X. Zhao, L. Deng, Application of ZrB2 thin film as a low emissivity film at high temperature, Appl. Surf. Sci. 527 (2020) 146763. https://doi.org/10.1016/j.apsusc.2020.146763.

[8] Z. Wang, C. Wang, H. Hou, W. Liu, R. Nian, H. Sun, X. Chen, G. Cui, A facile fabrication of stimulus-responsive amorphous photonic crystals in the near-infrared region, Appl. Surf. Sci. 479 (2019) 1014–1020. https://doi.org/10.1016/j.apsusc.2019.02.143.

[9] N. Liu, M. Mesch, T. Weiss, M. Hentschel, H. Giessen, Infrared perfect absorber and its application as plasmonic sensor, Nano Lett. 10 (2010) 2342–2348. https://doi.org/10.1021/nl9041033.

[10] H.-H. Chou, A. Nguyen, A. Chortos, J.W.F. To, C. Lu, J. Mei, T. Kurosawa, W.-G. Bae, J.B.-H. Tok, Z. Bao, A chameleon-inspired stretchable electronic skin with interactive colour changing controlled by tactile sensing, Nat. Commun. 6 (2015) 8011. https://doi.org/10.1038/ncomms9011.

[11] H. Kim, J. Choi, K.K. Kim, P. Won, S. Hong, S.H. Ko, Biomimetic chameleon soft robot with artificial crypsis and disruptive coloration skin, Nat. Commun. 12 (2021) 4658. https://doi.org/10.1038/s41467-021-24916-w.

[12] H. Liu, C. Wang, G. Chen, Y. Liao, M. Mao, T. Cheng, A. Libanori, X. Xiao, X. Hu, K. Liu, J. Chen, Moisture assisted photo-engineered textiles for visible and self-adaptive infrared dual camouflage, Nano Energy 93 (2022) 106855. https://doi.org/10.1016/j.nanoen.2021.106855.

[13] H. Feng, X. Li, M. Wang, F. Xia, K. Zhang, W. Kong, L. Dong, M. Yun, Ultrabroadband metamaterial absorbers from ultraviolet to near-infrared based on multiple resonances for harvesting solar energy, Opt. Exp., OE 29 (2021) 6000–6010. https://doi.org/10.1364/OE.419269.

[14] A. Lenert, D.M. Bierman, Y. Nam, W.R. Chan, I. Celanović, M. Soljačić, E.N. Wang, A nanophotonic solar thermophotovoltaic device, Nat. Nanotechnol. 9 (2014) 126–130. https://doi.org/10.1038/nnano.2013.286.

[15] F. Maremi, N. Lee, G. Choi, T. Kim, H. Cho, Design of Multilayer Ring Emitter Based on Metamaterial for Thermophotovoltaic Applications, Energies 11 (2018) 2299. https://doi.org/10.3390/en11092299.

[16] A.P. Raman, M.A. Anoma, L. Zhu, E. Rephaeli, S. Fan, Passive radiative cooling below ambient air temperature under direct sunlight, Nature 515 (2014) 540–544. https://doi.org/10.1038/nature13883.

[17] J. Wang, M. Shen, Z. Liu, W. Wang, MXene materials for advanced thermal management and thermal energy utilization, Nano Energy 97 (2022) 107177. https://doi.org/10.1016/j.nanoen.2022.107177.

[18] H.J. Kim, Y.H. Choi, D. Lee, I.H. Lee, B.K. Choi, S.-H. Phark, Y.J. Chang, Enhanced passive thermal stealth properties of VO2 thin films via gradient W doping, Appl. Surf. Sci. 561 (2021) 150056. https://doi.org/10.1016/j.apsusc.2021.150056.

[19] N. Lee, T. Kim, J.-S. Lim, I. Chang, H.H. Cho, Metamaterial-Selective Emitter for Maximizing Infrared Camouflage Performance with Energy Dissipation, ACS Appl. Mater. Interf. 11 (2019) 21250–21257. https://doi.org/10.1021/acsami.9b04478.

[20] N. Lee, J.-S. Lim, I. Chang, D. Lee, H.H. Cho, Flexible Thermocamouflage Materials in Supersonic Flowfields with Selective Energy Dissipation, ACS Appl. Mater. Interf. 13 (2021) 43524–43532. https://doi.org/10.1021/acsami.1c09333.

[21] N. Lee, J.-S. Lim, I. Chang, D. Lee, H.H. Cho, Transparent Metamaterials for Multispectral Camouflage Transparent Metamaterials for Multispectral Camouflage with Thermal Management, Int. J. Heat Mass Transf. 173 (2021) 121173.

[22] Y. Liu, Z. Feng, C. Xu, A. Chatterjee, A.A. Gorodetsky, Reconfigurable Micro- and Nano-Structured Camouflage Surfaces Inspired by Cephalopods, ACS Nano 15 (2021) 17299−17309. https://doi.org/10.1021/acsnano.0c09990.

[23] H. Zhu, Q. Li, C. Tao, Y. Hong, Z. Xu, W. Shen, S. Kaur, P. Ghosh, M. Qiu, Multispectral camouflage for infrared, visible, lasers and microwave with radiative cooling, Nat. Commun. 12 (2021) 1805. https://doi.org/10.1038/s41467-021-22051-0.

[24] Y. Cengel, Heat and mass transfer: fundamentals and applications, McGraw-Hill Higher Education, 2014.

[25] J. Lee, H. Sul, Y. Jung, H. Kim, S. Han, J. Choi, J. Shin, D. Kim, J. Jung, S. Hong, S.H. Ko, Thermally Controlled, Active Imperceptible Artificial Skin in Visible-to-Infrared Range, Adv. Funct. Mater. 30 (2020) 2003328. https://doi.org/10.1002/adfm.202003328.

[26] S. Hong, S. Shin, R. Chen, An Adaptive and Wearable Thermal Camouflage Device, Adv. Funct. Mater. 30 (2020) 1909788. https://doi.org/10.1002/adfm.201909788.

[27] P. Won, K.K. Kim, H. Kim, J.J. Park, I. Ha, J. Shin, J. Jung, H. Cho, J. Kwon, H. Lee, S.H. Ko, Imperceptible Soft Robotics: Transparent Soft Actuators/Sensors and Camouflage Skins for Imperceptible Soft Robotics (Adv. Mater. 19/2021), Adv. Mater. 33 (2021) 2170147. https://doi.org/10.1002/adma.202170147.

[28] P. Won, K.K. Kim, H. Kim, J.J. Park, I. Ha, J. Shin, J. Jung, H. Cho, J. Kwon, H. Lee, S.H. Ko, Transparent Soft Actuators/Sensors and Camouflage Skins for Imperceptible Soft Robotics, Adv. Mater. 33 (2021) e2002397. https://doi.org/10.1002/adma.202002397.

[29] N. Lee, B. Yoon, T. Kim, J.-Y. Bae, J.-S. Lim, I. Chang, H.H. Cho, Multiple Resonance Metamaterial Emitter for Deception of Infrared Emission with Enhanced Energy Dissipation, ACS Appl. Mater. Interf. 12 (2020) 8862–8869. https://doi.org/10.1021/acsami.9b21030.

[30] H. Zhu, Q. Li, C. Zheng, Y. Hong, Z. Xu, H. Wang, W. Shen, S. Kaur, P. Ghosh, M. Qiu, High-temperature infrared camouflage with efficient thermal management, Light Sci. Appl. 9 (2020) 60. https://doi.org/10.1038/s41377-020-0300-5.

[31] Y. Qu, Q. Li, L. Cai, M. Pan, P. Ghosh, K. Du, M. Qiu, Thermal camouflage based on the phase-changing material GST, Light Sci. Appl. 7 (2018) 26. https://doi.org/10.1038/s41377-018-0038-5.

[32] T. Kim, J.-Y. Bae, N. Lee, H.H. Cho, Hierarchical Metamaterials for Multispectral Camouflage of Infrared and Microwaves, Adv. Funct. Mater. 29 (2019) 1807319. https://doi.org/10.1002/adfm.201807319.

[33] A. Safaei, S. Chandra, M.N. Leuenberger, D. Chanda, Wide Angle Dynamically Tunable Enhanced Infrared Absorption on Large-Area Nanopatterned Graphene, ACS Nano 13 (2019) 421–428. https://doi.org/10.1021/acsnano.8b06601.

[34] M. Pan, Y. Huang, Q. Li, H. Luo, H. Zhu, S. Kaur, M. Qiu, Multi-band middle-infrared-compatible camouflage with thermal management via simple photonic structures, Nano Energy 69 (2020) 104449. https://doi.org/10.1016/j.nanoen.2020.104449.

[35] R.D. Hudson, Infrared system engineering, Wiley-Interscience, Hoboken, N.J., 1969 (2006 printing).

[36] D.P. Sheehan, Infrared Cloaking, Stealth, and the Second Law of Thermodynamics, Entropy 14 (2012) 1915–1938. https://doi.org/10.3390/e14101915.

[37] L. Peng, D. Liu, H. Cheng, S. Zhou, M. Zu, A Multilayer Film Based Selective Thermal Emitter for Infrared Stealth Technology, Adv. Opt. Mater. 6 (2018) 1801006. https://doi.org/10.1002/adom.201801006.

[38] J. Song, J. Seo, J. Han, J. Lee, B.J. Lee, Ultrahigh emissivity of grating-patterned PDMS film from 8 to 13 μ m wavelength regime, Appl. Phys. Lett. 117 (2020) 94101. https://doi.org/10.1063/5.0017838.

[39] Arsalan Razzaq, Valérie Depauw, Jinyoun Cho, Hariharsudan Sivaramakrishnan Radhakrishnan, Ivan Gordon, Jozef Szlufcik, Yaser Abdulraheem, Jef Poortmans, Periodic inverse nanopyramid gratings for light management in silicon heterojunction devices and comparison with random pyramid texturing, Solar Energy Mater. Solar Cells 206 (2020) 110263. https://doi.org/10.1016/j.solmat.2019.110263.

[40] R. Chen, M.-C. Lu, V. Srinivasan, Z. Wang, H.H. Cho, A. Majumdar, Nanowires for enhanced boiling heat transfer, Nano Lett. 9 (2009) 548–553. https://doi.org/10.1021/nl8026857.

[41] Donghwi Lee, Namkyu Lee, Dong Il Shim, Beom Seok Kim, Hyung Hee Cho, Enhancing thermal stability and uniformity in boiling heat transfer using micro-nano hybrid surfaces (MNHS), Appl. Therm. Eng. 130 (2018) 710–721. https://doi.org/10.1016/j.applthermaleng.2017.10.144.

[42] B.S. Kim, S.H. Tamboli, J.B. Han, T. Kim, H.H. Cho, Broadband radiative energy absorption using a silicon nanowire forest with silver nanoclusters for thermal energy conversion, Int. J. Heat Mass Transf. 82 (2015) 267–272. https://doi.org/10.1016/j.ijheatmasstransfer.2014.11.043.

[43] X. Zhu, Z. Zhang, X. Men, J. Yang, K. Wang, X. Xu, X. Zhou, Q. Xue, Robust superhydrophobic surfaces with mechanical durability and easy repairability, J. Mater. Chem. 21 (2011) 15793. https://doi.org/10.1039/c1jm12513c.

[44] G. Gong, K. Gao, J. Wu, N. Sun, C. Zhou, Y. Zhao, L. Jiang, A highly durable silica/polyimide superhydrophobic nanocomposite film with excellent thermal stability and abrasion-resistant performance, J. Mater. Chem. A 3 (2015) 713–718. https://doi.org/10.1039/C4TA04442H.

[45] C.-L. Xu, Y.-Z. Wang, Durability, anti-corrosion and self-clean in air/oil of a transparent superhydrophobic polyimide film, Appl. Mater. Today 10 (2018) 18–23. https://doi.org/10.1016/j.apmt.2017.11.008.

[46] M. Choi, S.H. Lee, Y. Kim, S.B. Kang, J. Shin, M.H. Kwak, K.-Y. Kang, Y.-H. Lee, N. Park, B. Min, A terahertz metamaterial with unnaturally high refractive index, Nature 470 (2011) 369–373. https://doi.org/10.1038/nature09776.

[47] J. Kischkat, S. Peters, B. Gruska, M. Semtsiv, M. Chashnikova, M. Klinkmüller, O. Fedosenko, S. Machulik, A. Aleksandrova, G. Monastyrskyi, Y. Flores, W.T. Masselink, Mid-infrared optical properties of thin films of aluminum oxide, titanium dioxide, silicon dioxide, aluminum nitride, and silicon nitride, Appl. Opt. 51 (2012) 6789–6798. https://doi.org/10.1364/AO.51.006789.

[48] N.W. Pech-May, L. Tobias, M. Retsch, Design of Multimodal Absorption in the Mid-IR: A Metal Dielectric Metal Approach, ACS Appl. Mater. Interf. 13 (2021) 1921–1929. https://doi.org/10.1021/acsami.0c18160.

[49] Dan Yang, Yufeng Ni, Hao Su, Yuxiang Shi, Qiming Liu, Xiangyu Chen, Deyan He, Hybrid energy system based on solar cell and self-healing/self-cleaning triboelectric nanogenerator, Nano Energy 79 (2021) 105394. https://doi.org/10.1016/j.nanoen.2020.105394.

[50] E. Hecht, Optics, Addison Wesley San Francisco, 2002.

[51] T. A. Kelf, Y. Sugawara, R. M. Cole, J. J. Baumberg, M. E. Abdelsalam, S. Cintra, S. Mahajan, A. E. Russell, P. N. Bartlett, Localized and delocalized plasmons in metallic nanovoids, Phys. Rev. B 74 (2006) 245415. https://doi.org/10.1103/PhysRevB.74.245415.

[52] Z.M. Zhang, G. Lefever-Button, F.R. Powell, Infrared Refractive Index and Extinction Coefficient of Polyimide Films, Int. J. Thermophys. 19 (1998) 905–916. https://doi.org/10.1023/A:1022655309574.

[53] A. Vora, J. Gwamuri, N. Pala, A. Kulkarni, J.M. Pearce, D.Ö. Güney, Exchanging Ohmic losses in metamaterial absorbers with useful optical absorption for photovoltaics, Sci. Rep. 4 (2014) 4901. https://doi.org/10.1038/srep04901.

[54] S. Derler, J. Süess, A. Rao, G.-M. Rotaru, Influence of variations in the pressure distribution on the friction of the finger pad, Tribol. Int. 63 (2013) 14–20. https://doi.org/10.1016/j.triboint.2012.03.001.